IEEE Access
The journal for rapid open access publishing

Received October 5, 2015, accepted October 21, 2015, date of current version November 10, 2015.

Digital Object Identifier 10.1109/ACCESS.2015.2494861

Extrinsic Information Transfer Charts for Characterizing the Iterative Decoding Convergence of Fully Parallel Turbo Decoders

HOANG ANH NGO, ROBERT G. MAUNDER, AND LAJOS HANZO
Department of Electronics and Computer Science, University of Southampton, Southampton SO17 1BJ, U.K.

Corresponding author: L. Hanzo (lh@ecs.soton.ac.uk)

This work was supported in part by the Engineering and Physical Sciences Research Council and in part by the European Research Council Advanced Fellow Grant.

ABSTRACT Fully parallel turbo decoders (FPTDs) have been shown to offer a more-than-sixfold processing throughput and latency improvement over the conventional logarithmic Bahl–Cocke–Jelinek–Raviv (Log-BCJR) turbo decoders. Rather than requiring hundreds or even thousands of time periods to decode each frame, such as the conventional Log-BCJR turbo decoders, the FPTD completes each decoding iteration using only one or two time periods, although up to six times as many decoding iterations are required to achieve the same error correction performance. Until now, it has not been possible to explain this increased iteration requirement using an extrinsic information transfer (EXIT) chart analysis, since the two component decoders are not alternately operated in the FPTD. Hence, in this paper, we propose a novel EXIT chart technique for characterizing the iterative exchange of not only extrinsic logarithmic likelihood ratios in the FPTD, but also the iterative exchange of extrinsic state metrics. In this way, the proposed technique can accurately predict the number of decoding iterations required for achieving iterative decoding convergence, as confirmed by the Monte Carlo simulation. The proposed technique offers new insights into the operation of FPTDs, which will facilitate improved designs in the future, in the same way as the conventional EXIT charts have enhanced the design and understanding of the conventional Log-BCJR turbo decoders.

INDEX TERMS Fully-parallel decoding, turbo code, EXIT chart.

I. INTRODUCTION

Turbo codes [1], [2] have been adopted for providing error correction in a number of advanced communication systems, such as the 3rd-Generation Wideband Code Division Multiple Access (3G WCDMA) [3], [4] and 4th-Generation Long Term Evolution (4G LTE) systems [5]. A turbo code comprises a parallel concatenation of two component convolutional codes. By iteratively exchanging soft information in the form of Logarithmic Likelihood Ratios (LLRs) [1] between the two corresponding component decoders, turbo codes facilitate reliable communication at transmission throughputs that approach the channel capacity [6], [7]. Conventional turbo decoders employ the Logarithmic Bahl-Cocke-Jelinek-Raviv (Log-BCJR) algorithm [8]. This is applied to the two convolutional codes alternately, until an error-free decoded frame is obtained or until the maximum number of decoding iterations is reached. However, the Log-BCJR algorithm has an inherently serial processing nature, owing to the data dependencies within its forward and backward recursions. This limits the processing throughput and latency of conventional turbo decoders, which imposes a bottleneck both on the transmission throughput and on the end-to-end latency in real-time communication systems. A number of techniques have been proposed for increasing the parallelism and hence improving both the processing throughput and latency of Log-BCJR turbo decoders. These solutions include shuffled iterative decoding [9], sub-block parallelism [10], [11], the Radix-4 transform [12] and the Non-Sliding Window (NSW) technique [12]. These techniques allow both recursions of both convolutional codes to be performed simultaneously, as well as allowing the recursions to consider several turbo-encoded bits per time period. However, in each case, the data dependencies of the forward and backward recursions require the turbo encoded bits of each convolutional code to be processed serially, spread over numerous consecutive time periods. As a result,

IEEE Access
The journal for rapid open access publishing

each decoding iteration requires hundreds or even thousands of processing time periods, hence limiting the processing throughput of the state-of-art turbo decoder [12] to 2.15 Gbit/s, which is far below the target of 10 Gbit/s in 5G [13].

Against this background, we previously proposed the Fully-Parallel Turbo Decoder (FPTD) algorithm [14], where all bits in the frame may be decoded in parallel, allowing each decoding iteration to be completed using just one or two time periods. This offers a more than six-fold processing throughput and latency improvement, over the state-of-the-art Log-BCJR turbo decoder, when employed for the LTE turbo code [14]. As a result, the FPTD facilitates both processing throughputs exceeding 10 Gbit/s and ultra-low processing latencies, hence satisfying the challenging requirements of 5G for the first time.

The number of decoding iterations required for conventional Log-BCJR turbo decoders to converge may be characterized by EXtrinsic Information Transfer (EXIT) chart analysis [15], which considers the iterative exchange of extrinsic Logarithmic Likelihood Ratios (LLRs) between the two component decoders. The EXIT charts have been extensively employed for analyzing the performance of the conventional binary error correction codes as well as of the future quantum ones [16]. Against this background, the new contributions of this paper are as follows:

1) We demonstrate that in addition to the extrinsic LLRs, the FPTD also iteratively exchanges extrinsic state metrics [14], which cannot be considered by conventional EXIT chart techniques. Instead, the FPTD must be considered as a system having multiple types of extrinsic information.
2) We analyse the inter-dependencies of these different types of extrinsic information and propose a novel technique for the EXIT chart analysis of the FPTD. In this way, the proposed technique can accurately predict the number of decoding iterations required for the FPTD to achieve iterative decoding convergence, as confirmed by Monte Carlo simulations. For the first time, the proposed technique reveals why the FPTD requires six times as many iterations as a conventional Log-BCJR turbo decoder, in order to achieve the same error correction performance. The proposed technique offers new insights into the operation of the FPTD, which will enable improved designs in the future, in the same way as conventional EXIT charts have enhanced the design and understanding of conventional Log-BCJR turbo decoders.
3) We propose a modification to conventional EXIT charts, in order to allow both the performance and characteristics of Log-BCJR turbo decoders to be compared with those of the FPTD.

The outline of the paper is as follows. Section II summarizes the FPTD algorithm, focusing on the aspects most relevant to this work. The new EXIT chart proposed for analysing the FPTD is detailed in Section III, followed in Section IV by our performance comparison between the Log-BCJR-based turbo decoder and the FPTD using the new EXIT chart analysis. Finally, our concluding remarks are offered in Section V.

II. FULLY-PARALLEL TURBO DECODER

The FPTD is compatible with any turbo encoder [1], including those of the 3G WCDMA and 4G LTE standards. In a turbo encoder [1], a message bit vector $\mathbf{b}_1^{\mathrm{u}} = [b_{1,k}^{\mathrm{u}}]_{k=1}^{N}$ comprising N number of bits is encoded by the upper convolutional encoder, generating the parity bit vector $\mathbf{b}_2^{\mathrm{u}} = [b_{2,k}^{\mathrm{u}}]_{k=1}^{N}$ and the systematic bit vector $\mathbf{b}_3^{\mathrm{u}} = [b_{3,k}^{\mathrm{u}}]_{k=1}^{N} = \mathbf{b}_1^{\mathrm{u}}$. Meanwhile, the message bit vector $\mathbf{b}_1^{\mathrm{u}}$ is interleaved in order to obtain the interleaved message bit vector $\mathbf{b}_1^{\mathrm{l}} = [b_{1,k}^{\mathrm{l}}]_{k=1}^{N}$ and then encoded by the lower convolutional encoder to produce the parity bit vector $\mathbf{b}_2^{\mathrm{l}} = [b_{2,k}^{\mathrm{l}}]_{k=1}^{N}$. Following this, the systematic bit vector $\mathbf{b}_3^{\mathrm{u}}$ and the parity bit vectors $\mathbf{b}_2^{\mathrm{u}}$ and $\mathbf{b}_2^{\mathrm{l}}$ are modulated and transmitted to the receiver.

At the receiver, the demodulator produces *a priori* soft information in the form of the LLR vectors $\bar{\mathbf{b}}_2^{\mathrm{u,a}}$, $\bar{\mathbf{b}}_2^{\mathrm{l,a}}$, $\bar{\mathbf{b}}_3^{\mathrm{u,a}}$ and $\bar{\mathbf{b}}_3^{\mathrm{l,a}}$, where the latter is obtained by interleaving $\bar{\mathbf{b}}_3^{\mathrm{u,a}}$. The *a priori* LLR vectors are input to the FPTD, which was detailed in [14]. Briefly, an FPTD comprises two fully parallel convolutional component decoders, as shown in Fig. 1. Each of the component decoders comprises N number of algorithmic blocks, as shown in Fig. 2. Note that in contrast to [14] where a systematic LLR vector $\bar{\mathbf{b}}_3^{\mathrm{u,a}}$ is only provided for the upper decoder, the FPTD of Fig. 1 and Fig. 2 has been modified to accept the systematic LLR vector $\bar{\mathbf{b}}_3^{\mathrm{l,a}}$ for the lower decoder for the sake of constructing symmetrical EXIT charts, as will be shown in Section III-C. This makes the FPTD symmetrical, allowing the superscripts $^{\mathrm{u}}$ and $^{\mathrm{l}}$ to

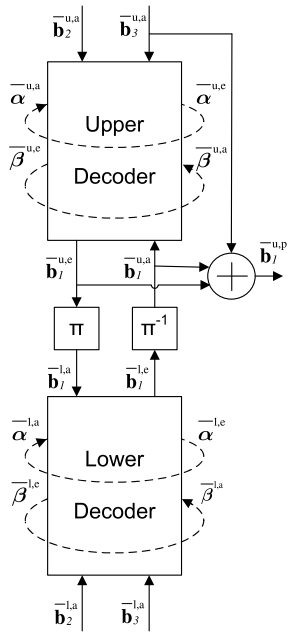

FIGURE 1. Block diagram of the FPTD.

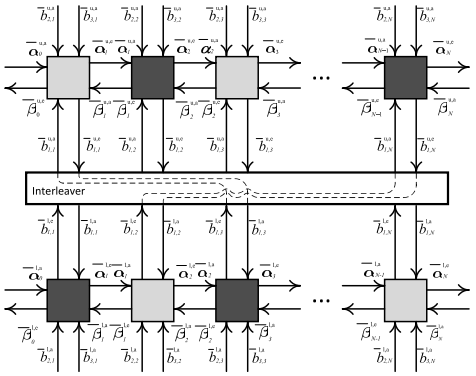

FIGURE 2. Schematic of the FPTD.

be omitted in the following discussions, wherever they apply equally to both the upper and lower decoders.

As illustrated in Fig. 1 and Fig. 2, the inputs of each component decoder comprise the *a priori* systematic LLR vector $\bar{\mathbf{b}}_3^{\mathrm{a}} = [\bar{b}_{3,k}^{\mathrm{a}}]_{k=1}^{N}$ and the *a priori* parity LLR vector $\bar{\mathbf{b}}_2^{\mathrm{a}} = [\bar{b}_{2,k}^{\mathrm{a}}]_{k=1}^{N}$ gleaned from the demodulator, the *a priori* message LLR vector $\bar{\mathbf{b}}_1^{\mathrm{a}} = [\bar{b}_{1,k}^{\mathrm{a}}]_{k=1}^{N}$ extracted from the other component decoder, the *a priori* forward state metric vectors $\bar{\boldsymbol{\alpha}}^{\mathrm{a}} = [\bar{\boldsymbol{\alpha}}_k^{\mathrm{a}}]_{k=0}^{N}$ and the *a priori* backward state metric vectors $\bar{\boldsymbol{\beta}}^{\mathrm{a}} = [\bar{\boldsymbol{\beta}}_k^{\mathrm{a}}]_{k=0}^{N}$ fed back from the previous iteration, where $\bar{\boldsymbol{\alpha}}_k^{\mathrm{a}} = [\bar{\alpha}_k^{\mathrm{a}}(S_k)]_{S_k=0}^{M-1}$, $\bar{\boldsymbol{\beta}}_k^{\mathrm{a}} = [\bar{\beta}_k^{\mathrm{a}}(S_k)]_{S_k=0}^{M-1}$ and M is the number of states in the corresponding state transition diagram [14]. Meanwhile, the outputs comprise the extrinsic message LLR vector $\bar{\mathbf{b}}_1^{\mathrm{e}} = [\bar{b}_{1,k}^{\mathrm{e}}]_{k=1}^{N}$ for the other decoder, as well as the forward state metric vectors $\bar{\boldsymbol{\alpha}}^{\mathrm{e}} = [\bar{\boldsymbol{\alpha}}_k^{\mathrm{e}}]_{k=0}^{N}$ and the backward state metric vectors $\bar{\boldsymbol{\beta}}^{\mathrm{e}} = [\bar{\boldsymbol{\beta}}_k^{\mathrm{e}}]_{k=0}^{N}$, which will be fed into to the next iteration, where $\bar{\boldsymbol{\alpha}}_k^{\mathrm{e}} = [\bar{\alpha}_k^{\mathrm{e}}(S_k)]_{S_k=0}^{M-1}$ and $\bar{\boldsymbol{\beta}}_k^{\mathrm{e}} = [\bar{\beta}_k^{\mathrm{e}}(S_k)]_{S_k=0}^{M-1}$

The FPTD operates in an iterative manner, spread over a series of consecutive time periods. In each time period, some or all of the $2N$ algorithmic blocks are operated in parallel. For turbo codes employing an arbitrary interleaver pattern, all $2N$ algorithmic blocks are operated in every time period. However, if the turbo code employs an odd-even interleaver [17], then the FPTD may employ an odd-even operation of the algorithm blocks [14]. More explicitly, an odd-even interleaver only connects algorithmic blocks from the upper row having an odd index to blocks from the lower row that also have an odd index. Similarly, the blocks from the upper row having an even index are only connected to those from the lower row also having an even index. This arrangement groups the $2N$ decoding blocks into two sets. The first set includes the odd-indexed blocks in the upper row and the even-indexed blocks in the lower row, which are indicated by the light grey shading in Fig. 2. Meanwhile, the second set comprises the even-indexed blocks in the upper row and the odd-indexed blocks in the lower row, which are indicated by the dark grey shading in Fig. 2. Given this arrangement, the FPTD may operate only the first set in odd indexed time periods and only the second set in even indexed time periods. This reduces the computational complexity of the FPTD by 50% without increasing the number of time periods required for completing the decoding process [14].

Whenever an algorithmic block is operated, it performs (2)-(5), as shown at the bottom of this page. Note that these equations have been modified relative to those of [14], in order to make the FPTD symmetrical, as described above. More specifically, the algorithmic block having the index k uses (2) to combine the *a priori* LLRs $\bar{b}_{1,k}^{\mathrm{a}}$, $\bar{b}_{2,k}^{\mathrm{a}}$ and $\bar{b}_{3,k}^{\mathrm{a}}$, as well as the *a priori* state metric vectors $\bar{\boldsymbol{\alpha}}_{k-1}^{\mathrm{a}}$ and $\bar{\boldsymbol{\beta}}_k^{\mathrm{a}}$ to produce an *a posteriori* state metric $\bar{\delta}(S_{k-1}, S_k)$ for each transition in the state transition diagram [14], namely for each pair of states S_{k-1} and S_k, for which it is possible for the convolutional encoder to traverse between, as indicated using the notation $c(S_{k-1}, S_k) = 1$. Here, $b_j(S_{k-1}, S_k)$ is the value that is implied for the bit $b_{j,k}$ by the transition between the state S_{k-1} and S_k, according to the state transition diagram [14]. These *a posteriori* transition metrics are then combined by (3)-(5), in order to produce the extrinsic forward state metric vector $\bar{\boldsymbol{\alpha}}_k^{\mathrm{e}} = [\bar{\alpha}_k^{\mathrm{e}}(S_k)]_{S_k=0}^{M-1}$, the extrinsic backward state metric vector $\bar{\boldsymbol{\beta}}_{k-1}^{\mathrm{e}} = [\bar{\beta}_{k-1}^{\mathrm{e}}(S_{k-1})]_{S_{k-1}=0}^{M-1}$ and the extrinsic LLR $\bar{b}_{1,k}^{\mathrm{e}}$, respectively. These equations employ the Jacobian logarithm, which is defined for two operands as

$$\max^*(\bar{\delta}_1, \bar{\delta}_2) = \max(\bar{\delta}_1, \bar{\delta}_2) + \ln\left(1 + e^{-|(\bar{\delta}_1 - \bar{\delta}_2)|}\right), \quad (1)$$

$$\bar{\delta}(S_{k-1}, S_k) = \left[\sum_{j=1}^{3}[b_j(S_{k-1}, S_k) \cdot \bar{b}_{j,k}^{\mathrm{a}}]\right] + \bar{\alpha}_{k-1}^{\mathrm{a}}(S_{k-1}) + \bar{\beta}_k^{\mathrm{a}}(S_k), \quad (2)$$

$$\bar{\alpha}_k^{\mathrm{e}}(S_k) = \left[\max^*_{\{S_{k-1}|c(S_{k-1},S_k)=1\}}[\bar{\delta}(S_{k-1}, S_k)]\right] - \bar{\beta}_k^{\mathrm{a}}(S_k) = \max^*_{\{S_{k-1}|c(S_{k-1},S_k)=1\}}\left[\sum_{j=1}^{3}[b_j(S_{k-1}, S_k) \cdot \bar{b}_{j,k}^{\mathrm{a}}] + \bar{\alpha}_{k-1}^{\mathrm{a}}(S_{k-1})\right], \quad (3)$$

$$\bar{\beta}_{k-1}^{\mathrm{e}}(S_{k-1}) = \left[\max^*_{\{S_k|c(S_{k-1},S_k)=1\}}[\bar{\delta}(S_{k-1}, S_k)]\right] - \bar{\alpha}_{k-1}^{\mathrm{a}}(S_{k-1}) = \max^*_{\{S_{k-1}|c(S_{k-1},S_k)=1\}}\left[\sum_{j=1}^{3}[b_j(S_{k-1}, S_k) \cdot \bar{b}_{j,k}^{\mathrm{a}}] + \bar{\beta}_k^{\mathrm{a}}(S_k)\right], \quad (4)$$

$$\bar{b}_{1,k}^{\mathrm{e}} = \left[\max^*_{\{(S_{k-1},S_k)|b_1(S_{k-1},S_k)=1\}}[\bar{\delta}(S_{k-1}, S_k)]\right] - \left[\max^*_{\{(S_{k-1},S_k)|b_1(S_{k-1},S_k)=0\}}[\bar{\delta}(S_{k-1}, S_k)]\right] - \bar{b}_{1,k}^{\mathrm{a}} - \bar{b}_{3,k}^{\mathrm{a}}. \quad (5)$$

IEEE Access
The journal for rapid open access publishing

and may be extended to more operands by exploiting its associativity property. Following the final decoding iteration, an *a posteriori* LLR pertaining to the k^{th} message bit $b^{\text{u}}_{1,k}$ may be obtained as $\bar{b}^{\text{u,p}}_{1,k} = \bar{b}^{\text{u,e}}_{1,k} + \bar{b}^{\text{u,a}}_{1,k} + \bar{b}^{\text{u,a}}_{3,k}$. A hard decision for the message bit $b^{\text{u}}_{1,k}$ may then be obtained as the result of the binary test $\bar{b}^{\text{u,p}}_{1,k} > 0$.

In summary, the operation of the FPTD differs for that of the conventional BCJR-based turbo decoding in a number of ways, which prevent conventional EXIT chart analysis. In particular, some or all of the $2N$ algorithmic blocks are operated in parallel in the FPTD. More specifically, when an odd-even interleaver is employed, the iterative decoding process alternates between the operation of two odd-even sets of algorithmic blocks, rather than between the upper and lower component decoders, as in a conventional turbo decoder. Furthermore, the extrinsic forward state metric vectors $\bar{\boldsymbol{\alpha}}^{\text{e}}$ and the extrinsic backward state metric vectors $\bar{\boldsymbol{\beta}}^{\text{e}}$ are fed back in the FPTD and used as the *a priori* information $\bar{\boldsymbol{\alpha}}^{\text{a}}$ and $\bar{\boldsymbol{\beta}}^{\text{a}}$ in the next time period, as shown in Fig. 1.

III. EXIT CHART OF FULLY-PARALLEL TURBO DECODING

As described in Section II, the FPTD employs not only an iterative exchange of extrinsic LLRs between algorithmic blocks, but additionally exchanging extrinsic state metric vectors. By contrast, classic EXIT charts [15], [18] are designed to consider only the LLRs, and hence they are unable to consider the state metric vectors. More specifically, in conventional turbo decoders [1] and EXIT charts, each component decoder outputs only extrinsic LLRs and these depend only on the input *a priori* LLRs. But in the FPTD, each algorithmic block outputs an extrinsic LLR $\bar{b}^{\text{e}}_{1,k}$ and two extrinsic state metric vectors $\bar{\boldsymbol{\beta}}^{\text{e}}_{k-1}$ and $\bar{\boldsymbol{\alpha}}^{\text{e}}_{k}$, which depend on the input *a priori* LLR $\bar{b}^{\text{a}}_{1,k}$ and *a priori* state metric vectors $\bar{\boldsymbol{\alpha}}^{\text{a}}_{k-1}$ and $\bar{\boldsymbol{\beta}}^{\text{a}}_{k}$. Therefore, it is impossible to characterize the performance of a fully-parallel decoder using the conventional EXIT chart [7]. Motivated by this, the dependence of the algorithmic blocks' various sets of output extrinsic information upon their various sets of input *a priori* information will be examined in this section. Furthermore, a novel EXIT chart technique will be proposed for characterizing the performance of the FPTD.

In order to support the analysis of this section, an $M = 8$-state LTE turbo code [5] having a coding rate of 1/3, a frame length of $N = 6144$ bits and trellis termination is employed as an example. Additionally, Binary Phase Shift Keying (BPSK) modulation is assumed for communication over a Rayleigh fading channel [19].

A. MUTUAL INFORMATION

In order to characterize the relationships between each algorithmic block's input as well as output LLRs and the state metric vectors, their quality can be quantified by their Mutual Information (MI) [20], [21], as discussed in the following sub-sections.

1) MUTUAL INFORMATION OF LLRs

The MI of LLRs was analysed in [18], [21], and [20]. More particularly, the MI $I(\bar{\mathbf{b}}^{\text{a}}_1)$ of the *a priori* message LLR vector $\bar{\mathbf{b}}^{\text{a}}_1$ may be formulated using [18, eq. (12)]. Meanwhile, the MI $I(\bar{\mathbf{b}}^{\text{e}}_1)$ of the extrinsic message LLR vector $\bar{\mathbf{b}}^{\text{e}}_1$ may be quantified using (19) of [18]. Note that since an LLR vector contains information pertaining to a binary vector, its MI will be in the range of 0 to 1, where 0 represents no information and 1 represents perfect information. Conventional EXIT charts [15], [18] characterize the MI of extrinsic LLR vector as functions of the MI of *a priori* LLR vectors. This is achieved by generating artificial *a priori* message LLR vectors $\bar{\mathbf{b}}^{\text{a}}_1$ having a particular MI $I(\bar{\mathbf{b}}^{\text{e}}_1)$ and then measuring the MI $I(\bar{\mathbf{b}}^{\text{e}}_1)$ of the extrinsic message LLR vectors $\bar{\mathbf{b}}^{\text{e}}_1$ that result from processing these inputs. The process of generating artificial *a priori* message LLR vectors was detailed in [18].

2) MUTUAL INFORMATION OF STATE METRIC VECTORS

The MI of the extrinsic forward state metric vectors $\bar{\boldsymbol{\alpha}}^{\text{e}}$ may be calculated as [22]:

$$I(\bar{\boldsymbol{\alpha}}^{\text{e}}) = \log_2(M) - \frac{1}{N}\sum_{k=1}^{N}\sum_{S_k=0}^{M-1} P[\bar{\alpha}^{\text{e}}_k(S_k)] \times \log_2\left(\frac{1}{P[\bar{\alpha}^{\text{e}}_k(S_k)]}\right) \in [1, \log_2(M)], \tag{6}$$

where the probability $P[\bar{\alpha}^{\text{e}}_k(S_k)]$ associated with the extrinsic state metric $\bar{\alpha}^{\text{e}}_k(S_k)$ may be calculated as

$$P[\bar{\alpha}^{\text{e}}_k(S_k)] = \frac{\exp\left[\bar{\alpha}^{\text{e}}_k(S_k)\right]}{\sum_{S'_k=0}^{M-1}\exp\left[\bar{\alpha}^{\text{e}}_k(S'_k)\right]}. \tag{7}$$

As described in Section II, the extrinsic state metric vectors $\bar{\boldsymbol{\alpha}}^{\text{e}}$ contain information pertaining to M states $S_k \in [0, M-1]$. Owing to this, the MI of state metric vectors ranges from 0 to $\log_2(M)$. Similarly, the MI of the extrinsic backward state metric vectors $\bar{\boldsymbol{\beta}}^{\text{e}}$ may be calculated using (6).

In previous work on non-binary EXIT charts [22], the techniques used for generating artificial *a priori* metrics imposed correlation between the metrics that does not reflect the correlation typically exhibited between the *a priori* metrics obtained during iterative decoding. In this paper we propose a novel technique for generating sets of uncorrelated *a priori* state metric vectors $\bar{\boldsymbol{\alpha}}^{\text{a}}$ and $\bar{\boldsymbol{\beta}}^{\text{a}}$ having particular MI $I(\bar{\boldsymbol{\alpha}}^{\text{a}})$ and $I(\bar{\boldsymbol{\beta}}^{\text{a}})$. We begin by mapping each element $\bar{\alpha}^{\text{a}}_k(S_k)$ or $\bar{\beta}^{\text{a}}_k(S_k)$ of each state metric vector to one of M constellation points within an M-dimensional space. The S_k^{th} constellation point $Q(S_k)$ has a unity value for the coordinate in the S_k^{th} dimension and zero values for the coordinates in the other $(M-1)$ dimensions, where $S_k \in [0, M-1]$. The vector of states selected during the conventional encoding process $\boldsymbol{S} = [S_k]_{k=1}^{N}$ is mapped to the corresponding vector of these M-dimensional constellation points $\mathbf{Q} = [Q(S_k)]_{k=1}^{N}$. Following this, we generate a vector of N random M-dimensional Gaussian distributed noise elements $\boldsymbol{n} = [n_k]_{k=1}^{N}$ having an M-dimensional variance of unity.

Next we adjust the standard deviation σ of the noise $\boldsymbol{n}$ and add it to the vector of selected constellation points $\mathbf{Q}$, according to

$$\boldsymbol{y} = \mathbf{Q} + \sigma \times \boldsymbol{n}, \tag{8}$$

where $\boldsymbol{y} = [y_k]_{k=1}^{N}$. Following this, the *a priori* state metric $\bar{\alpha}_k^{\mathrm{a}}(S_k)$ becomes proportional to the Euclidean distance between y_k and the constellation point $Q(S_k)$, according to

$$\bar{\alpha}_k^{\mathrm{a}}(S_k) = \frac{||y_k - Q(S_k)||^2}{2\sigma^2}, \tag{9}$$

where $||\cdot||$ is the M-dimensional norm. Finally, we measure the MI of $\bar{\boldsymbol{\alpha}}^{\mathrm{a}}$ using (6) and use trial and error to adjust the standard deviation σ, until the desired MI is obtained.

Note however that the above-described technique generates *a priori* state metric vectors $\bar{\boldsymbol{\alpha}}^{\mathrm{a}}$ and $\bar{\boldsymbol{\beta}}^{\mathrm{a}}$ within which there is no correlation. More specifically, if a particular incorrect state metric $\bar{\alpha}_k^{\mathrm{e}}(S_k)$ has a high value, this does not make it more likely that any other particular incorrect state metric $\bar{\alpha}_k^{\mathrm{e}}(S_k')$ in the vector $\bar{\boldsymbol{\alpha}}_k^{\mathrm{e}}$ will also have a high value. In practice, however, some correlation is exhibited within the *a priori* state metric vectors, particularly during the early iterations. This leads to some inaccuracy between the predictions made by our novel EXIT chart technique and the true values, as will be discussed in Section III-F. Our future work will consider the modeling of this correlation, although we expect that this will significantly increase the complexity of the EXIT chart technique, while only marginally improving its accuracy.

B. THE RELATIONSHIP BETWEEN THE A PRIORI AND EXTRINSIC INFORMATION

According to (3), the value of each extrinsic forward state metric $\bar{\alpha}_k^{\mathrm{e}}(S_k)$ in a particular iteration depends on the incoming *a priori* LLRs $\bar{b}_{1,k}^{\mathrm{a}}$, $\bar{b}_{2,k}^{\mathrm{a}}$ and $\bar{b}_{3,k}^{\mathrm{a}}$, as well as on the value of the *a priori* forward state metrics in the vector $\bar{\boldsymbol{\alpha}}_{k-1}^{\mathrm{a}}$ fed back from the previous iteration. Similarly, the value of each extrinsic backward state metric $\bar{\beta}_{k-1}^{\mathrm{e}}(S_{k-1})$ depends both on the incoming *a priori* LLRs $\bar{b}_{1,k}^{\mathrm{a}}$, $\bar{b}_{2,k}^{\mathrm{a}}$ and $\bar{b}_{3,k}^{\mathrm{a}}$, as well as on the value of the *a priori* backward state metrics in the vector $\bar{\boldsymbol{\beta}}_k^{\mathrm{a}}$ fed back from the previous iteration, according to (4). Moreover, since they are provided by the demodulator, the quality of the LLRs $\bar{b}_{2,k}^{\mathrm{a}}$ and $\bar{b}_{3,k}^{\mathrm{a}}$ depends upon the specific E_b/N_0 value of the channel. Hence, the MI of the extrinsic state metric vectors may be formulated as

$$I(\bar{\boldsymbol{\alpha}}^{\mathrm{e}}) = f_\alpha\big[I(\bar{\boldsymbol{\alpha}}^{\mathrm{a}}), I(\bar{\mathbf{b}}_1^{\mathrm{a}}), E_b/N_0\big] \in \big[0, \log_2(M)\big], \tag{10}$$

and

$$I(\bar{\boldsymbol{\beta}}^{\mathrm{e}}) = f_\beta\big[I(\bar{\boldsymbol{\beta}}^{\mathrm{a}}), I(\bar{\mathbf{b}}_1^{\mathrm{a}}), E_b/N_0\big] \in \big[0, \log_2(M)\big], \tag{11}$$

where $M = 8$ is the number of states in the LTE turbo code.

By contrast, it may be seen from (2) and (5) that the extrinsic LLR $\bar{b}_{1,k}^{\mathrm{e}}$ depends both on the *a priori* forward state metrics in the vector $\bar{\boldsymbol{\alpha}}_{k-1}^{\mathrm{a}}$ and the *a priori* backward state metrics in the vector $\bar{\boldsymbol{\beta}}_k^{\mathrm{a}}$ fed back from the previous iteration, as well as on the *a priori* parity LLR $\bar{b}_{2,k}^{\mathrm{a}}$, which depends on E_b/N_0. Hence, the MI of the LLR vector $\bar{\mathbf{b}}_1^{\mathrm{e}}$ can be presented as:

$$I(\bar{\mathbf{b}}_1^{\mathrm{a}}) = f_b\big[I(\bar{\boldsymbol{\alpha}}^{\mathrm{a}}), I(\bar{\boldsymbol{\beta}}^{\mathrm{a}}), E_b/N_0\big] \in \big[0, 1\big]. \tag{12}$$

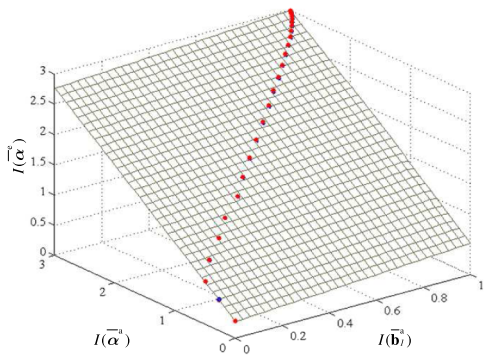

FIGURE 3. Surface plot of $I(\bar{\alpha}^{\mathrm{e}}) = f_\alpha\big[I(\bar{\alpha}^{\mathrm{a}}), I(\bar{\mathbf{b}}_1^{\mathrm{a}}), E_b/N_0\big]$ for the case where an LTE turbo code [5] having a frame length of $N = 6144$ bits is employed with BPSK modulation for communication over a Rayleigh fading channel having $E_b/N_0 = 4$ dB.

C. EXIT FUNCTIONS

Fig. 3 provides a surface plot of (10) for the LTE turbo decoder, when using BPSK modulation for communication over a Rayleigh fading channel having $E_b/N_0 = 4$ dB. This surface plot characterizes the dependence f_α of the MI of the extrinsic forward state metric vector $I(\bar{\boldsymbol{\alpha}}^{\mathrm{e}})$ upon both the MI of the *a priori* LLR vector $I(\bar{\mathbf{b}}_1^{\mathrm{a}})$ and on the MI of the *a priori* forward state metric vectors $I(\bar{\boldsymbol{\alpha}}^{\mathrm{a}})$. The *a priori* message LLR vector $\bar{\mathbf{b}}_{1,k}^{\mathrm{a}}$ was generated using the Gaussian process presented in [18], while the *a priori* forward state metric vectors $\bar{\boldsymbol{\alpha}}_k^{\mathrm{a}}$ were generated using the Gaussian non-binary process detailed in Section III-A.

In Fig. 3 the bold dots represent the combinations of $I(\bar{\boldsymbol{\alpha}}^{\mathrm{e}})$, $I(\bar{\boldsymbol{\alpha}}^{\mathrm{a}})$ and $I(\bar{\mathbf{b}}_1^{\mathrm{a}})$ that were measured during the successive time periods of the iterative operation of the LTE FPTD. Fig. 3 shows that the measured points are coincident with the surface plot. Hence, it may be concluded that the EXIT surface of Fig. 3 is in agreement with the measured simulation results. It may also be observed from the measurements of Fig. 3 that in the first $\log_2(M) = 3$ time periods, the *a priori* message LLRs have a MI $I(\bar{\mathbf{b}}_1^{\mathrm{a}})$ of almost zero, increasing only marginally, despite the MI of the state metric vectors $I(\bar{\boldsymbol{\alpha}}^{\mathrm{e}})$ and $I(\bar{\boldsymbol{\alpha}}^{\mathrm{a}})$ increasing significantly. This may be explained by the correlation within the *a priori* forward state metric vectors that is exhibited during the early iterations, as described in Section III-A. This correlation results in similar $\bar{\delta}(S_{k-1}, S_k)$ values for the transitions in the trellis having $b_1(S_{k-1}, S_k) = 0$ and $b_1(S_{k-1}, S_k) = 1$, giving extrinsic LLRs $\bar{b}_{1,k}^{\mathrm{e}}$ having low values, according to (2).

Similarly, a surface plot of (11) may be used for characterizing the dependence f_β of the MI of the extrinsic backward state metric vectors $I(\bar{\boldsymbol{\beta}}^{\mathrm{e}})$ both on the MI of the incoming *a priori* LLR vector $I(\bar{\mathbf{b}}_1^{\mathrm{a}})$ and on the MI of the *a priori* backward state metric vectors $I(\bar{\boldsymbol{\beta}}^{\mathrm{a}})$. However, the resultant

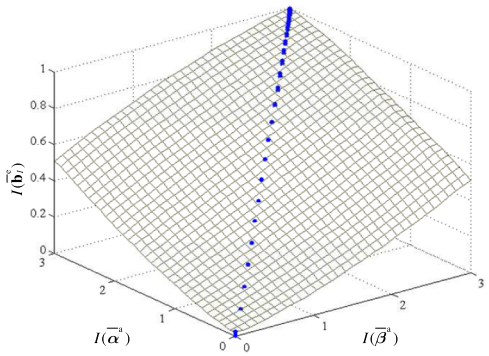

FIGURE 4. Surface plot of $I(\bar{b}_1^{\mathrm{e}}) = f_b[I(\bar{\alpha}^{\mathrm{a}}), I(\bar{\beta}^{\mathrm{a}}), E_b/N_0]$ for the case where an LTE turbo code [5] having a frame length of $N = 6144$ bits is employed with BPSK modulation for communication over a Rayleigh fading channel having $E_b/N_0 = 4$ dB.

surface plot is indistinguishable from Fig. 3 in the case of LTE turbo code and hence it is omitted from this paper.

Fig. 4 provides a surface plot of (12) for the LTE turbo code, characterizing the relationship f_b between the MI of the extrinsic LLR vector $I(\bar{\mathbf{b}}_1^{\mathrm{e}})$ with the MI of the forward state metric vectors $I(\bar{\boldsymbol{\alpha}}^{\mathrm{a}})$ and the MI of the backward state metric vectors $I(\bar{\boldsymbol{\beta}}^{\mathrm{a}})$. Again, the values of $\bar{\boldsymbol{\alpha}}^{\mathrm{a}}$ and $\bar{\boldsymbol{\beta}}^{\mathrm{a}}$ are generated and their MI is measured using the processes described in Section III-A. Here, the bold dots represent combinations of $I(\bar{\mathbf{b}}_1^{\mathrm{e}})$, $I(\bar{\boldsymbol{\alpha}}^{\mathrm{a}})$ and $I(\bar{\boldsymbol{\beta}}^{\mathrm{a}})$ that were measured during successive time periods during the iterative operation of the LTE FPTD. Again, an agreement between the EXIT surface plot and the measured simulation results is also found in Fig. 4.

D. EXIT CHART TRAJECTORY

As analysed in Sections III-B and III-C, the relationship between the inputs and outputs of the algorithmic blocks of a FPTD may be characterized by the corresponding EXIT functions. By combining the EXIT functions in an EXIT chart, we may predict the evolution of the extrinsic information exchanged between the algorithmic blocks as the iterative decoding process proceeds. This information can be visualized as a decoding trajectory in the EXIT chart, which allows us to characterise the number of decoding time periods required by the FPTD to achieve iterative decoding convergence.

Therefore, this section focuses on the procedure of plotting the trajectory for the EXIT chart of the FPTD. More particularly, the algorithm to produce the EXIT trajectory is detailed as follows:

- **Step 1**: Plot the MI of the extrinsic forward state metric vectors $I(\bar{\boldsymbol{\alpha}}^{\mathrm{e}}) = f_\alpha\big[I(\bar{\boldsymbol{\alpha}}^{\mathrm{a}}), I(\bar{\mathbf{b}}_1^{\mathrm{a}}), E_b/N_0\big]$ and extrinsic LLRs $I(\bar{\mathbf{b}}_1^{\mathrm{e}}) = f_b\big[I(\bar{\boldsymbol{\alpha}}^{\mathrm{a}}), E_b/N_0\big]$ in the same set of three axes, labelled as $I(\bar{\boldsymbol{\alpha}}^{\mathrm{a}})/I(\bar{\boldsymbol{\beta}}^{\mathrm{a}})$, $I(\bar{\boldsymbol{\alpha}}^{\mathrm{e}})/I(\bar{\boldsymbol{\beta}}^{\mathrm{e}})$ and $I(\bar{\mathbf{b}}_1^{\mathrm{a}})/I(\bar{\mathbf{b}}_1^{\mathrm{e}})$. Note that as detailed in Section III-C, f_α and f_β are identical and hence it is only necessary to plot one of them. Also plot the diagonal plane, where we have $I(\bar{\boldsymbol{\alpha}}^{\mathrm{a}}) = I(\bar{\boldsymbol{\alpha}}^{\mathrm{e}})$, as shown in Fig. 5.
- **Step 2**: To represent the start of the decoding process, set the initial MI of the *a priori* forward state metrics $I(\bar{\boldsymbol{\alpha}}^{\mathrm{a}})$, the extrinsic forward state metrics $I(\bar{\boldsymbol{\alpha}}^{\mathrm{e}})$ and the *a priori* LLRs $I(\bar{\mathbf{b}}_1^{\mathrm{e}})$ to zero, according to $\big[I^0(\bar{\boldsymbol{\alpha}}^{\mathrm{a}}), I^0(\bar{\boldsymbol{\alpha}}^{\mathrm{e}}), I^0(\bar{\mathbf{b}}_1^{\mathrm{a}})\big] = (0, 0, 0)$.

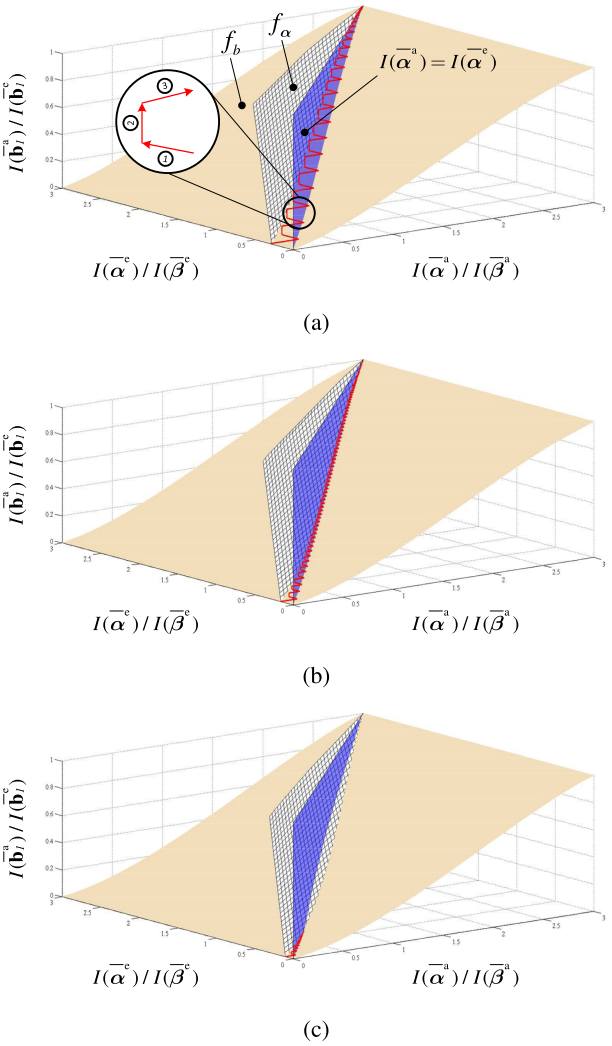

FIGURE 5. 3D EXIT charts of the FPTD at different E_b/N_0 values. A LTE $M = 8$-state turbo code [5] having a coding rate of 1/3 is employed along with BPSK modulation for communication over a Rayleigh fading channel. (a) $E_b/N_0 = 4.0$ dB. (b) $E_b/N_0 = 1.8$ dB. (c) $E_b/N_0 = 0.0$ dB.

- **Step 3**: Plot the EXIT trajectory, which is demonstrated in Fig. 5a as follows,
  - 1. Starting from the point $\big[I^{i-1}(\bar{\boldsymbol{\alpha}}^{\mathrm{a}}), I^{i-1}(\bar{\boldsymbol{\alpha}}^{\mathrm{e}}), I^{i-1}(\bar{\mathbf{b}}_1^{\mathrm{a}})\big]$, project along the $I(\bar{\boldsymbol{\alpha}}^{\mathrm{e}})/I(\bar{\boldsymbol{\beta}}^{\mathrm{e}})$ axis, until the extrinsic forward state metric surface f_α is met at $[I^{i-1}(\bar{\boldsymbol{\alpha}}^{\mathrm{a}}), I^{i}(\bar{\boldsymbol{\alpha}}^{\mathrm{e}}), I^{i-1}(\bar{\mathbf{b}}_1^{\mathrm{a}})]$, where we have $I^{i}(\bar{\boldsymbol{\alpha}}^{\mathrm{e}}) = f_\alpha\big[I^{i-1}(\bar{\boldsymbol{\alpha}}^{\mathrm{a}}), I^{i-1}(\bar{\mathbf{b}}_1^{\mathrm{a}}), E_b/N_0\big]$, as shown using ① in Fig. 5a. This step represents the calculation of (3) and (4) within the algorithmic blocks.
  - 2. Starting from the point $\big[I^{i-1}(\bar{\boldsymbol{\alpha}}^{\mathrm{a}}), I^{i}(\bar{\boldsymbol{\alpha}}^{\mathrm{e}}), I^{i-1}(\bar{\mathbf{b}}_1^{\mathrm{a}})\big]$, project along the $I(\bar{\boldsymbol{b}}_1^{\mathrm{a}})/I(\bar{\boldsymbol{b}}_1^{\mathrm{e}})$ axis, until the extrinsic LLR vector surface is met at $\big[I^{i-1}(\bar{\boldsymbol{\alpha}}^{\mathrm{a}}), I^{i}(\bar{\boldsymbol{\alpha}}^{\mathrm{e}}), I^{i}(\bar{\mathbf{b}}_1^{\mathrm{e}})\big]$, where we have $I^{i}(\bar{\mathbf{b}}_1^{\mathrm{e}}) = f_b\big[I^{i-1}(\bar{\boldsymbol{\alpha}}^{\mathrm{a}}), E_b/N_0\big]$, as shown using ② in Fig. 5a.

This step represents the calculation of (5) within the algorithmic blocks. Note that the algorithmic blocks perform (5) simultaneously with (3) and (4). However, since the $I^i(\bar{\mathbf{b}}_1^{\mathrm{e}})$ value calculated in this step is independent of the $I^i(\bar{\boldsymbol{\alpha}}^{\mathrm{e}})$ value calculated in step 3.1, it makes no difference if the two steps are performed successively, rather than simultaneously.

– 3. Commencing from the point $\left[I^{i-1}(\bar{\boldsymbol{\alpha}}^{\mathrm{a}}), I^i(\bar{\boldsymbol{\alpha}}^{\mathrm{e}}), I^i(\bar{\mathbf{b}}_1^{\mathrm{e}})\right]$, project along the $I(\bar{\boldsymbol{\alpha}}_1^{\mathrm{a}})$ axis until the diagonal plane is met at $\left(I^i(\bar{\boldsymbol{\alpha}}^{\mathrm{a}}), I^i(\bar{\boldsymbol{\alpha}}^{\mathrm{e}}), I^i(\bar{\mathbf{b}}_1^{\mathrm{a}})\right)$, where $I^i(\bar{\boldsymbol{\alpha}}^{\mathrm{a}}) = I^i(\bar{\boldsymbol{\alpha}}^{\mathrm{e}})$ and $I^i(\bar{\mathbf{b}}_1^{\mathrm{a}}) = I^i(\bar{\boldsymbol{b}}_1^{\mathrm{e}})$, as shown using ③ in Fig. 5a. This step represents the mechanism by which the extrinsic information generated by a particular algorithmic block is used as *a priori* information by the connected blocks in the next time period.

- **Step 4**: Repeat Step 3 for each time period i, plotting a point in the EXIT chart for each combination of $\left[I^i(\bar{\boldsymbol{\alpha}}^{\mathrm{a}}), I^i(\bar{\boldsymbol{\alpha}}^{\mathrm{e}}), I^i(\bar{\mathbf{b}}_1^{\mathrm{a}})\right]$ obtained, as shown in Fig. 5.

E. ITERATIVE DECODING CONVERGENCE

Inspired by our previous work on 3D EXIT charts [23], [24], the iterative decoding convergence of the FPTD may be characterized by the open tunnel and the convergence point in the 3D EXIT chart presented in Section III-D. More particularly, the convergence point is located at the first intersection between the extrinsic state metric vector surface $I(\bar{\boldsymbol{\alpha}}^{e}) = f_\alpha\left[I(\bar{\boldsymbol{\alpha}}^{\mathrm{a}}), I(\bar{\mathbf{b}}_1^{\mathrm{a}}), E_b/N_0\right]$, the extrinsic LLR surface $I(\bar{\boldsymbol{b}}_1^{\mathrm{e}}) = f_b\left[I(\bar{\boldsymbol{\alpha}}^{\mathrm{a}}), E_b/N_0\right]$ and the diagonal plane $I(\bar{\boldsymbol{\alpha}}^{\mathrm{a}}) = I(\bar{\boldsymbol{\alpha}}^{\mathrm{e}})$. When the convergence point is located at the $\left[I^\infty(\bar{\boldsymbol{\alpha}}^{\mathrm{a}}), I^\infty(\bar{\boldsymbol{\alpha}}^{\mathrm{e}}), I^\infty(\bar{\mathbf{b}}_1^{\mathrm{a}})\right] = (3, 3, 1)$ point of the 3D EXIT chart, the tunnel is considered to be open. By contrast, a closed tunnel is obtained if the convergence point is located below (3, 3, 1). The wider the open tunnel, the fewer time periods are required for achieving iterative decoding convergence. When the tunnel is open, a relatively low BER may be achieved. Meanwhile, a closed tunnel results in a high BER, regardless of how many time periods are used during the iterative decoding process. This observation is similar to the convergence trends of a conventional EXIT chart [7], [18], where a low BER is achieved, when the convergence point is located at the (1,1) point, forming an open tunnel between the two EXIT functions.

The convergence is characterized for the scenario where the LTE FPTD is used for communication over a Rayleigh channel having different E_b/N_0 values in Fig. 5. As shown in Fig. 5c, at $E_b/N_0 = 0$ dB the EXIT tunnel is closed and the FPTD converges to a point below the (3,3,1) point. By contrast, at the threshold of $E_b/N_0 = 1.8$ dB the EXIT tunnel becomes narrowly open in Fig. 5b, facilitating a low BER. However, the trajectory seen in Fig. 6b comprises a high number of plotted points, indicating that a large number of time periods are required to reach the (3,3,1) point. Meanwhile, a significantly lower number of decoding iterations is required at $E_b/N_0 = 4$ dB, where a broadly-open tunnel is achieved in Fig. 5a.

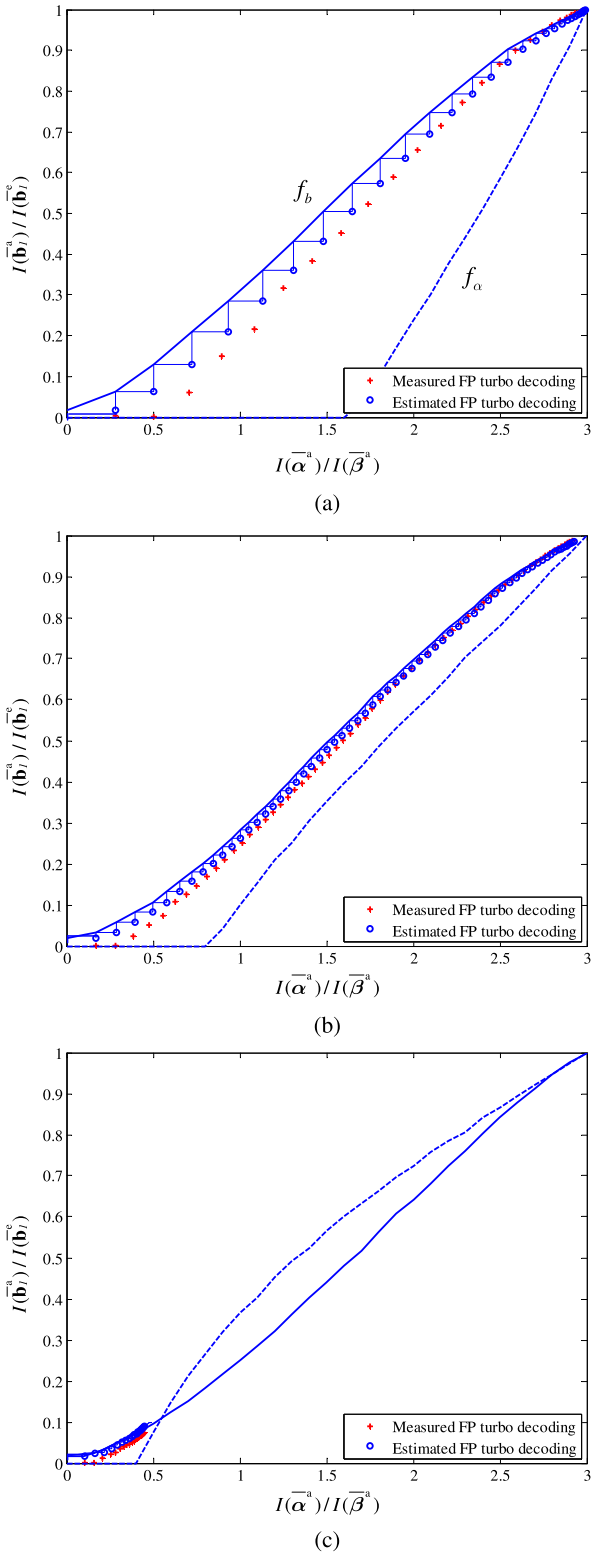

FIGURE 6. 2D EXIT charts of the FPTD at different E_b/N_0 values. A LTE $M = 8$-state turbo code [5] having a coding rate of 1/3 is employed along with BPSK modulation for communication over a Rayleigh fading channel. (a) $E_b/N_0 = 4.0$ dB. (b) $E_b/N_0 = 1.8$ dB. (c) $E_b/N_0 = 0.0$ dB.

F. PROJECTION INTO TWO DIMENSIONS

The 3D EXIT chart of Section III-D offers an insight into the performance of the FPTD. However, a 3D plot is inconvenient

both for visualizing the iterative decoding convergence and for quantifying the number of time periods required. Therefore, in this section we project the 3D EXIT chart into two dimensions for the sake of allowing a clearer observation. In particular, the 2D EXIT chart allows the improvement of MI after each time period to be clearly observed, whilst facilitating comparison with the Log-BCJR turbo decoder, as will be detailed in Section IV.

A 2D EXIT chart for the FPTD can be obtained by observing the diagonal $I(\bar{\boldsymbol{\alpha}}^{\mathrm{a}}) = I(\bar{\boldsymbol{\alpha}}^{\mathrm{e}})$ plane detailed from a view point parallel to the $I(\boldsymbol{\alpha}^{\mathrm{e}})$ axis. The 2D EXIT chart version of Fig. 5 is provided in Fig. 6. Here, the circular markers represent the projected 2D version of the simulations of Fig. 5, while the plus markers denote the measured MI observed after each time period of an decoding iteration for a single $N = 6144$-bit frame. Furthermore, the intersection between the diagonal $I(\bar{\boldsymbol{\alpha}}^{\mathrm{a}}) = I(\bar{\boldsymbol{\alpha}}^{\mathrm{e}})$ surface and the extrinsic LLR function f_b is shown using a continuous line, while the intersection between the diagonal and the extrinsic state metric functions f_α/f_β is shown using a dashed line. The position of the intersection between these two curves indicates whether the EXIT tunnel is open or closed, accordingly. Explicitly, an open EXIT chart tunnel is created in Fig. 6a and 6b, since these curve do not cross each other before reaching the $(I(\bar{\boldsymbol{\alpha}}^{\mathrm{a}}), I(\bar{\mathbf{b}}_1^{\mathrm{a}})) = (3, 1)$ point. By contrast, the curves do cross each other near the point (0.5, 0.1) in Fig. 6c, indicating that the tunnel is closed.

As shown in Fig. 6, there is some mismatch between the stage-case-shaped decoding trajectory points predicted by the simulations of Section III-E and those obtained by measuring the MIs observed after each time period during the iterative decoding of a single $N = 6144$-bit frame, i.e. between the circles and noses. This mismatch is particularly pronounced at the E_b/N_0 values of 4 dB and 1.8 dB considered in Fig. 6a and 6b. It is also more pronounced in the early stages of the iterative decoding process, below abscissa values of becoming successively reduced in successive time periods. However, it may be observed that there is a one-to-one match between the simulated and measured trajectory points, indicating that the proposed EXIT chart analysis correctly identifies the number of iterative decoding time periods required for achieving convergence. Note that the mismatch may be explained by the correlation that observed between the vectors of *a priori* state metrics $\bar{\boldsymbol{\alpha}}^{\mathrm{a}}$ and $\bar{\boldsymbol{\beta}}^{\mathrm{a}}$, which is not modelled by the process of Section III-A. As described in Section III-A, our future work will consider the modelling of the correlation, although separate analysis and modelling will be required for each time period of the FPTD iterative decoding process, hence significantly increasing the complexity of the analysis. While this would improve the match between the simulated and measured trajectory points, it would not improve the characterization of how many time periods are required to achieve iterative decoding convergence, since this is already accurate.

The achievable accuracy may be confirmed by comparing the 2D EXIT chart of Fig. 6a to the BER results of Fig. 7. Fig. 6a shows that around 32 time periods are required for achieving iterative decoding convergence to the $(I(\bar{\boldsymbol{\alpha}}^{\mathrm{a}}), I(\bar{\mathbf{b}}_1^{\mathrm{a}})) = (3, 1)$ point at $E_b/N_0 = 4.0$ dB. This corresponds to 16 iterations, since each iteration of the LTE FPTD comprises two time periods. This agrees with Fig. 7, which demonstrates that 16 iterations are required for achieving a BER below 10^{-5} at $E_b/N_0 = 4.0$ dB. Likewise, Fig. 6b shows that 64 time periods are required at $E_b/N_0 = 1.8$ dB, which requires 32 iterations required in Fig. 7. Likewise, both Fig. 6c and Fig. 7 show that iterative decoding convergence to a low BER is impossible for $E_b/N_0 = 0.0$ dB.

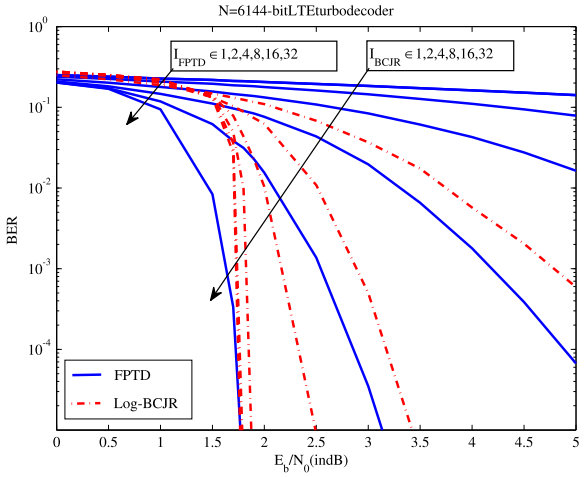

FIGURE 7. BER of the FPTD and Log-BCJR turbo decoders. A LTE $M = 8$-state turbo code [5] having a coding rate of 1/3 and a frame length of $N = 6144$ bits is employed along with BPSK modulation for communication over a Rayleigh fading channel. Plots are provided for the case where $I_{\mathrm{FPTD}} \in \{1, 2, 4, 8, 16, 32\}$ decoding iterations are performed using the FPTD, while $I_{\mathrm{BCJR}} \in \{1, 2, 4, 8, 16, 32\}$ decoding iterations are performed using the Log-BCJR turbo decoder.

IV. COMPARISON OF FULLY-PARALLEL AND LOG-BCJR TURBO DECODERS USING EXIT CHARTS

The novel 2D EXIT chart of Section III-F facilitates the characterization of the performance of the FPTD. However, it is noted that the horizontal axis of our 2D EXIT chart represents the MI of *a priori* state metric vectors, while the EXIT chart of conventional Log-BCJR turbo decoders represent the MI of LLRs on both axes [15], [18]. As a result, it is not trivial to use EXIT charts to compare the performance of the FPTD to that of the conventional Log-BCJR turbo decoder. However, in this section we show that this comparison can be achieved by modifying the EXIT charts of Log-BCJR turbo decoders to use the same axes as the novel EXIT chart of Section III-F.

A. MODIFICATION OF CONVENTIONAL EXIT CHARTS

In Log-BCJR turbo decoders, each component decoder employs the incoming *a priori* LLRs $\bar{\mathbf{b}}_1^{\mathrm{a}}$ in each iteration to compute the forward and backward state metrics $\bar{\boldsymbol{\alpha}}$ and $\bar{\boldsymbol{\beta}}$, which are then used for computing the extrinsic LLRs $\bar{\mathbf{b}}_1^{\mathrm{e}}$. Owing to this, the MI of the forward and backward state metrics can be considered to be a function of the MI of the

incoming *a priori* LLRs, according to

$$I(\bar{\boldsymbol{\alpha}}) = f_{\alpha}^{\mathrm{BCJR}}\left[I(\bar{\mathbf{b}}_1^{\mathrm{a}}), E_b/N_0\right] \in \left[0, \log_2(M)\right], \quad (13)$$

$$I(\bar{\boldsymbol{\beta}}) = f_{\beta}^{\mathrm{BCJR}}\left[I(\bar{\mathbf{b}}_1^{\mathrm{a}}), E_b/N_0\right] \in \left[0, \log_2(M)\right]. \quad (14)$$

In the case of the LTE turbo decoder, f_α and f_β are identical, in analogy to (10) and (11), as described in Section II. Meanwhile, the MI of the extrinsic LLRs is a function of the MI of the forward and backward state metrics, in analogy to (12) according to

$$\begin{aligned} I(\bar{\boldsymbol{b}}_1) &= f_b^{\mathrm{BCJR}}\left[I(\bar{\boldsymbol{\alpha}}), I(\bar{\boldsymbol{\beta}}), E_b/N_0\right] \\ &= f_b^{\mathrm{BCJR}}\left[I(\bar{\boldsymbol{\alpha}}), E_b/N_0\right] \in \left[0, 1\right]. \end{aligned} \quad (15)$$

Note that the forward and backward state metrics are calculated as intermediate variables, when converting the *a priori* LLRs $\bar{\mathbf{b}}_1^{\mathrm{a}}$ into the extrinsic LLRs $\bar{\mathbf{b}}_1^{\mathrm{e}}$. Owing to this, $I(\bar{\boldsymbol{\alpha}})$ is not considered in the conventional EXIT chart [15], [18], where only the MI functions $I(\bar{\mathbf{b}}_1^{\mathrm{a}})$ and $I(\bar{\mathbf{b}}_1^{\mathrm{e}})$ of the *a priori* and extrinsic LLRs are presented.

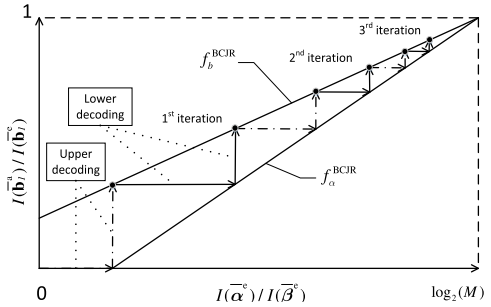

FIGURE 8. Modified EXIT chart.

However, a Log-BCJR turbo decoder may be characterized using an EXIT chart having the same axes, as in Fig. 6. The EXIT chart comprises two EXIT functions, namely f_α^{BCJR} and f_b^{BCJR}, as shown in Fig. 8. This exploits the observation that the extrinsic LLRs provided by one component decoder become the *a priori* LLRs for the other component decoder, giving $I(\bar{\mathbf{b}}_1^{\mathrm{a}}) = I(\bar{\mathbf{b}}_1^{\mathrm{e}})$ and allowing the Log-BCJR turbo decoder's operation to be characterized by the computation of f_α and f_b. Each iteration corresponds to two pairs of the horizontal and vertical trajectory steps. As illustrated in Fig. 8, the dashed trajectory steps correspond to the upper decoder, while the continuous trajectory steps correspond to the lower decoder. Additionally, the horizontal steps represent f_α of (13) while the vertical ones represent f_b of (15). Consequently, the modified Log-BCJR EXIT chart is equivalent to the novel design proposed for the FPTD in Section III.

B. EXIT CHART COMPARISON

By using the modified Log-BCJR EXIT chart of Section IV-A and the novel 2D EXIT chart of Section III-F, it is possible to compare the performance of the FPTD and the conventional Log-BCJR turbo decoder without the requirement for time consuming BER simulations.

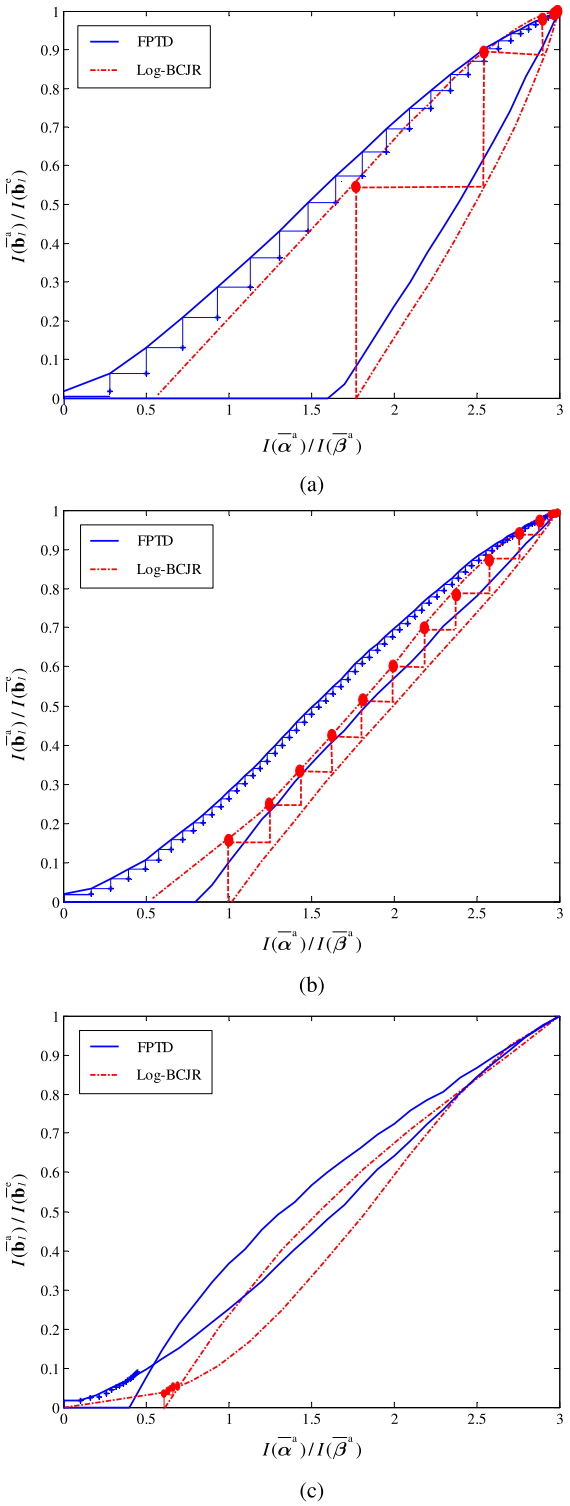

FIGURE 9. EXIT chart comparison between the FPTD and the Log-BCJR turbo decoder for various E_b/N_0 values. A LTE $M = 8$-state turbo code [5] having a coding rate of 1/3 and a frame length of $N = 6144$ bits is employed along with BPSK modulation for communication over a Rayleigh fading channel. (a) $E_b/N_0 = 4.0$ dB. (b) $E_b/N_0 = 1.8$ dB. (c) $E_b/N_0 = 0.0$ dB.

Fig. 9 shows the 2D EXIT chart of the FPTD and the Log-BCJR turbo decoder at $E_b/N_0 = 4.0$ dB, 1.8 dB and 0.0 dB. In this figure, each pairs of plus markers in the

FPTD EXIT trajectory corresponds to one of the decoding iterations, while each pair of circle markers in the Log-BCJR EXIT trajectory corresponds to one decoding iteration.

It may be observed from Fig. 9a that the FPTD requires 16 iterations to achieve iterative decoding convergence at $E_b/N_0 = 4.0$ dB, while the Log-BCJR turbo decoder requires only 2 iterations, as confirmed by the BER results of Fig. 7. When the EXIT tunnel is narrowly open at $E_b/N_0 = 1.8$ dB, the FPTD requires about 32 iterations, while the Log-BCJR turbo decoder requires 8 iterations to converge, as seen in Fig. 9b and confirmed by Fig. 7. By contrast, Fig. 9c shows the scenario, where the EXIT tunnels of both the FPTD and the Log-BCJR are closed at $E_b/N_0 = 0.0$ dB. This is confirmed by a high BER of about 0.2 at $E_b/N_0 = 0.0$ dB in Fig. 7, even if a high number of iterations are employed by both the FPTD and the Log-BCJR turbo decoder.

V. CONCLUSIONS

In this paper, we have proposed a novel EXIT chart, which allows the iterative decoding convergence of the FPTD to be characterized for the first time. We commenced by characterising the relationship between the inputs and outputs of each algorithmic block in the FPTD. A novel 3D EXIT chart was formulated for considering the MIs of both LLRs and state metrics. The proposed 3D EXIT chart was projected into two dimensions for clearer visualization and for allowing comparison with the Log-BCJR turbo decoder. By employing the EXIT chart, it was shown that an LTE FPTD having a frame length of $N = 6144$ requires 32 iterations at $E_b/N_0 = 1.8$ dB and 16 iterations at $E_b/N_0 = 4$ dB in order to achieve a low BER below 10^{-5}, which was confirmed by BER simulation measurements. The proposed techniques offer new insights into the operation of the FPTD, which will enable improved designs in the future, in the same way as conventional EXIT charts have enhanced the design and understanding of conventional Log-BCJR turbo decoders.

Based on the benefits of irregular coding [25], [26], our future work will consider the employment of the EXIT chart analysis proposed in this paper for designing *irregular* fully-parallel turbo codes. These codes will employ different state-transition diagrams in different subsets of the fully-parallel turbo decoders algorithmic blocks. Each different state-transition diagram can be expected to result in a different EXIT chart characteristic. Our future work will investigate how these different characteristics may be combined in order to obtain the overall EXIT chart characteristic of the irregular fully-parallel turbo decoder. We will then use this analysis to select which subsets of the algorithmic blocks should employ which state-transition diagrams, in order to create an overall EXIT chart characteristic that offers an open tunnel at the lowest channel SNR. In this way, we will facilitate near-capacity fully-parallel iterative decoding.

REFERENCES

[1] C. Berrou, A. Glavieux, and P. Thitimajshima, "Near Shannon limit error-correcting coding and decoding: Turbo-codes," in *Proc. IEEE Int. Conf. Commun. (ICC)*, vol. 2. Geneva, Switzerland, May 1993, pp. 1064–1070.

[2] M. Brejza, L. Li, R. Maunder, B. Al-Hashimi, C. Berrou, and L. Hanzo, "20 years of turbo coding and energy-aware design guidelines for energy-constrained wireless applications," *IEEE Commun. Surveys Tuts.*, to be published. [Online]. Available: http://ieeexplore.ieee.org/xpl/articleDetails.jsp?arnumber=7131434

[3] (2001). *3GPP Specifications Series. 25: Radio Aspects 3G, Including UMTS, The 3rd Generation Partnership Project (3GPP) Unites Telecommunications Standards Bodies*. [Online]. Available: http://www.3gpp.org/ftp/Specs/html-info/25-series.htm

[4] L.-N. Lee, A. R. Hammons, Jr., F.-W. Sun, and M. Eroz, "Application and standardization of turbo codes in third-generation high-speed wireless data services," *IEEE Trans. Veh. Technol.*, vol. 49, no. 6, pp. 2198–2207, Nov. 2000.

[5] *ETSI TS 136 212 LTE; Evolved Universal Terrestrial Radio Access (E-UTRA); Multiplexing Channel Coding*, ETSI, Route des Lucioles, France, 2013.

[6] J. P. Woodard and L. Hanzo, "Comparative study of turbo decoding techniques: An overview," *IEEE Trans. Veh. Technol.*, vol. 49, no. 6, pp. 2208–2233, Nov. 2000.

[7] L. L. Hanzo, T. H. Liew, B. L. Yeap, R. Y. S. Tee, and S. X. Ng, *Turbo Coding, Turbo Equalisation and Space-Time Coding: EXIT-Chart-Aided Near-Capacity Designs for Wireless Channels*. New York, NY, USA: Wiley, 2010.

[8] P. Robertson, E. Villebrun, and P. Hoeher, "A comparison of optimal and sub-optimal MAP decoding algorithms operating in the log domain," in *Proc. IEEE Int. Conf. Commun. (ICC)*, vol. 2. Seattle, WA, USA, Jun. 1995, pp. 1009–1013.

[9] J. Zhang and M. P. C. Fossorier, "Shuffled iterative decoding," *IEEE Trans. Commun.*, vol. 53, no. 2, pp. 209–213, Feb. 2005.

[10] O. Muller, A. Baghdadi, and M. Jézéquel, "Exploring parallel processing levels for convolutional turbo decoding," in *Proc. 2nd Int. Conf. Inf. Commun. Technol. (ICTTA)*, vol. 2. 2006, pp. 2353–2358.

[11] O. Muller, A. Baghdadi, and M. Jézéquel, "From parallelism levels to a multi-ASIP architecture for turbo decoding," *IEEE Trans. Very Large Scale Integr. (VLSI) Syst.*, vol. 17, no. 1, pp. 92–102, Jan. 2009.

[12] T. Ilnseher, F. Kienle, C. Weis, and N. Wehn, "A 2.15 GBit/s turbo code decoder for LTE advanced base station applications," in *Proc. 7th Int. Symp. Turbo Codes Iterative Inf. Process. (ISTC)*, Gothenburg, Sweden, Aug. 2012, pp. 21–25.

[13] R. El Hattachi, Ed., *5G White Paper*, 1st ed. Frankfurt, Germany: Next Generation Mobile Networks Alliance, Feb. 2015.

[14] R. G. Maunder, "A fully-parallel turbo decoding algorithm," *IEEE Trans. Commun.*, vol. 63, no. 8, pp. 2762–2775, Aug. 2015.

[15] S. ten Brink, "Convergence of iterative decoding," *Electron. Lett.*, vol. 35, no. 10, pp. 806–808, May 1999.

[16] Z. Babar, P. Botsinis, D. Alanis, S. X. Ng, and L. Hanzo, "The road from classical to quantum codes: A hashing bound approaching design procedure," *IEEE Access*, vol. 3, pp. 146–176, Mar. 2015. [Online]. Available: http://ieeexplore.ieee.org/xpl/articleDetails.jsp?arnumber=7052310

[17] A. Nimbalker, Y. Blankenship, B. Classon, and T. K. Blankenship, "ARP and QPP interleavers for LTE turbo coding," in *Proc. IEEE Wireless Commun. Netw. Conf. (WCNC)*, Mar./Apr. 2008, pp. 1032–1037.

[18] S. ten Brink, "Convergence behavior of iteratively decoded parallel concatenated codes," *IEEE Trans. Commun.*, vol. 49, no. 10, pp. 1727–1737, Oct. 2001.

[19] J. G. Proakis, *Digital Communications*, 4th ed. New York, NY, USA: McGraw-Hill, 2001.

[20] R. W. Hamming, *Coding and Information Theory*. Englewood Cliffs, NJ, USA: Prentice-Hall, 1986.

[21] T. M. Cover and J. A. Thomas, *Elements of Information Theory*. New York, NY, USA: Wiley, 1991.

[22] J. Kliewer, S. X. Ng, and L. Hanzo, "On the computation of EXIT characteristics for symbol-based iterative decoding," in *Proc. 4th Int. Symp. Turbo Codes Rel. Topics*, Apr. 2006, pp. 1–6.

[23] R. G. Maunder and L. Hanzo, "Extrinsic information transfer analysis and design of block-based intermediate codes," *IEEE Trans. Veh. Technol.*, vol. 60, no. 3, pp. 762–770, Mar. 2011.

[24] W. Zhang, Y. Jia, X. Meng, M. F. Brejza, R. G. Maunder, and L. Hanzo, "Adaptive iterative decoding for expediting the convergence of unary error correction codes," *IEEE Trans. Veh. Technol.*, vol. 64, no. 2, pp. 621–635, Feb. 2015.
[25] R. G. Maunder, J. Wang, S. X. Ng, L.-L. Yang, and L. Hanzo, "On the performance and complexity of irregular variable length codes for near-capacity joint source and channel coding," *IEEE Trans. Wireless Commun.*, vol. 7, no. 4, pp. 1338–1347, Apr. 2008.
[26] R. G. Maunder and L. Hanzo, "Near-capacity irregular variable length coding and irregular unity rate coding," *IEEE Trans. Wireless Commun.*, vol. 8, no. 11, pp. 5500–5507, Nov. 2009.

HOANG ANH NGO received the B.Eng. (Hons.) degree in electronics engineering from the Hanoi University of Science and Technology (HUST), Vietnam, in 2007, and the M.Sc. and Ph.D. degrees in wireless communications from the University of Southampton, U.K., in 2008 and 2012, respectively. From 2012 to 2014, he was with the Viettel Institute of Research and Development, Vietnam. Since 2014, he has been a Research Fellow with the University of Southampton. His research interests include co-located and distributed MIMO communications, space-time coding and modulation, and channel coding and modeling. He is a recipient of several academic awards from HUST, the University of Southampton, and the Engineering and Physical Sciences Research Council, U.K.

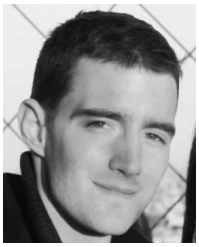

ROBERT G. MAUNDER has been with the Department of Electronics and Computer Science, University of Southampton, U.K., since 2000. He was awarded a first class honors B.Eng. in electronic engineering in 2003, and the Ph.D. in wireless communications in 2007. He became a Lecturer in 2007 and an Associated Professor in 2013. His research interests include joint source/channel coding, iterative decoding, irregular coding, and modulation techniques. For further information on this research, please refer to users.ecs.soton.ac.uk/rm.

LAJOS HANZO received the degree in electronics in 1976, the Ph.D. degree in 1983, and the Doctor Honoris Causa degree from the Technical University of Budapest, in 2009. During his 38-year career in telecommunications, he has held various research and academic positions in Hungary, Germany, and U.K. Since 1986, he has been with the School of Electronics and Computer Science, University of Southampton, U.K., as the Chair in Telecommunications. He has successfully supervised about 100 Ph.D. students, co-authored 20 John Wiley/IEEE Press books in mobile radio communications totaling in excess of 10 000 pages, authored over 1500 research entries at the IEEE Xplore, acted as the TPC Chair and General Chair of the IEEE conferences, presented keynote lectures, and received a number of distinctions. He is directing 100 strong academic research teams, working on a range of research projects in the field of wireless multimedia communications sponsored by the industry, the Engineering and Physical Sciences Research Council, U.K., the European Research Council's Advanced Fellow Grant, and the Royal Society's Wolfson Research Merit Award. He is an enthusiastic supporter of industrial and academic liaison and offers a range of industrial courses.

He is a fellow of the Royal Academy of Engineering, the Institution of Engineering and Technology, and the European Association for Signal Processing. He is also a Governor of the IEEE VTS. From 2008 to 2012, he was the Editor-in-Chief of the *IEEE Press* and a Chaired Professor with Tsinghua University, Beijing. He has over 22 000 citations.